Ultrasensitive, self-calibrated cavity ring-down spectrometer for quantitative trace gas analysis

Bing Chen,[1] Yu R. Sun,[1] Ze-Yi Zhou,[2] Jian Chen,[1] An-Wen Liu,[1] and Shui-Ming Hu[1,*]

[1]Hefei National Laboratory for Physical Sciences at Microscale, University of Science and Technology of China, Hefei 230026 China

[2]National Institute of Metrology, Beijing 100013, China

*Corresponding author: smhu@ustc.edu.cn

Received 19 August 2014; accepted 7 October 2014;
posted 13 October 2014 (Doc. ID 221202); published 6 November 2014

A cavity ring-down spectrometer is built for trace gas detection using telecom distributed feedback (DFB) diode lasers. The longitudinal modes of the ring-down cavity are used as frequency markers without active-locking either the laser or the high-finesse cavity. A control scheme is applied to scan the DFB laser frequency, matching the cavity modes one by one in sequence and resulting in a correct index at each recorded spectral data point, which allows us to calibrate the spectrum with a relative frequency precision of 0.06 MHz. Besides the frequency precision of the spectrometer, a sensitivity (noise-equivalent absorption) of 4×10^{-11} cm^{-1} Hz$^{-1/2}$ has also been demonstrated. A minimum detectable absorption coefficient of 5×10^{-12} cm^{-1} has been obtained by averaging about 100 spectra recorded in 2 h. The quantitative accuracy is tested by measuring the CO_2 concentrations in N_2 samples prepared by the gravimetric method, and the relative deviation is less than 0.3%. The trace detection capability is demonstrated by detecting CO_2 of ppbv-level concentrations in a high-purity nitrogen gas sample. Simple structure, high sensitivity, and good accuracy make the instrument very suitable for quantitative trace gas analysis.

OCIS codes: (120.6200) Spectrometers and spectroscopic instrumentation; (300.6340) Spectroscopy, infrared; (300.6360) Spectroscopy, laser.

http://dx.doi.org/10.1364/AO.53.007716

1. Introduction

Quantitative gas analysis by optical methods is widely applied in environmental monitoring [1,2], medical diagnosis [3], industrial process control [4], and security inspection [5]. In the last two decades, significant progress has been achieved using tunable lasers operating in the infrared (IR) [6], including diode lasers [3,7], quantum cascade lasers [2,8–10], optical parametric oscillators [11,12], difference frequency generation systems [13], and frequency combs [14]. Applications based on telecom distributed feedback (DFB) lasers (1.3–1.6 μm) are of particular interest because of their maturity, low cost, and convenient operation in both the lasers and detectors. The loss in molecular absorption due to shifting from strong fundamental bands in the mid-IR to weak overtones in the near-IR can be compensated for using cavity-enhanced techniques to increase the effective absorption path length [15]. Cavity ring-down spectroscopy (CRDS), as a method detecting the absorption spectrum, offers path lengths of hundreds of kilometers and a measurement of the absolute concentration of target species if the absorption cross section is known. As a result, trace gas detection with CRDS has attracted more and more interest in recent years [16].

1559-128X/14/327716-08$15.00/0

The sensitivity of a CRDS instrument is limited by the minimum detectable change in the cavity loss, usually expressed as the noise-equivalent absorption. In the pioneer implementations of CRDS using pulsed lasers [17], due to simultaneous excitation of multiple longitudinal modes of the cavity, the sensitivity was limited to $\sim 10^{-8}$ cm^{-1} Hz$^{-1/2}$ [18]. The sensitivity of CRDS based on continuous-wave (cw) lasers has been dramatically improved to $\sim 10^{-10}$ cm^{-1} Hz$^{-1/2}$ in the last decade [19–24]. Because of the narrow bandwidth nature of cw lasers, cw-CRDS also allows measurements with a resolution better than 0.001 cm^{-1}.

In a cw-CRDS measurement for quantitative analysis, one needs to match the laser frequency (width <10 MHz) to a longitudinal mode (typical width of ~1 kHz) of the high-finesse ring-down (RD) cavity, and also to determine either the scanning laser frequency or the resonant frequencies of the cavity modes. Note that the frequency precision, at least the relative one, is essential for quantitative measurements. For a Doppler-broadened line with a width of about 0.01 cm^{-1}, it is necessary to calibrate the spectrum to a precision of 0.0001 cm^{-1} to obtain a relative accuracy of 1% in the determined line intensity, since the observed line intensity is proportional to the product of the height and width of the line. One method is to sweep the cavity length repeatedly passing the resonance ("scanning cavity"), using a precise wavemeter or etalon to monitor the laser frequency. The method was first introduced by Romanini and his colleagues [25,26], and then became commonly applied in succeeding cw-CRDS studies, for example, in [16,21,27–30]. Using a similar experimental configuration and a RD cavity with a finesse of 4×10^5, Kassi and Campargue [23] recently obtained a sensitivity of 3×10^{-11} cm^{-1} Hz$^{-1/2}$. They demonstrated a minimum detectable absorption coefficient (MDAC) of 5×10^{-13} cm^{-1} by averaging over 6000 spectra recorded in 5 days, which is the best reported sensitivity of CRDS based on DFB lasers. In their experiments, a high-precision wavemeter was used to monitor the frequency of the slowly scanning laser. As a result, the frequency accuracy was limited both by the linewidth (~2 MHz) of the DFB laser and by the precision of the wavemeter (~10 MHz). We have established more precise spectral scanning using sidebands produced by an electro-optic modulator and a frequency-locked laser as the carrier [31]. However, sophisticated locking control and considerably higher cost are obstacles for trace-detection applications.

Alternatively, one can also periodically scan the laser frequency to match the longitudinal modes of the RD cavity ("scanning laser"), and the frequencies of the cavity modes can be used as a ruler to calibrate the spectrum [32–34]. Since tens or hundreds of cavity modes are involved in a scan, it is necessary to distinguish the cavity mode on resonance at each data point, which means to correctly index the data points. Incorrect indices of the data points introduce significant errors in calibration. However, it is not a trivial task in practice. For example, temperature fluctuations and mechanical vibrations lead to drifts and jitters on the frequencies of the cavity modes [35]. Chandler and Strecker recently presented a "dual-cavity" method for high-resolution measurements using a pulsed laser [36]. Hodges and his coworkers have established a frequency-stabilized CRDS by locking the cavity length to a He–Ne laser and also locking the probing laser (a single-mode external cavity diode laser, ECDL) to a specific longitudinal mode of the RD cavity [37]. Sophisticated locking control has been applied to establish a stepwise scan over successive modes of the RD cavity [38]. Recently, they have achieved a sensitivity of 2×10^{-12} cm^{-1} Hz$^{-1/2}$ using a narrow-linewidth (<100 Hz) ECDL laser, but the sensitivity degraded to 6×10^{-10} cm^{-1} Hz$^{-1/2}$ when a DFB laser with a linewidth of 2 MHz was used [24].

Here we present a CRDS instrument based on telecom DFB diode lasers using the "scanning laser" method. An automatic control scheme is applied to realize a strictly mode-by-mode scan over each of the cavity modes without active-locking either the laser or the cavity. It allows us to calibrate the spectrum recorded in each scan using the free spectral range (FSR) of the RD cavity. Despite the broad linewidth and tuning nonlinearity of the DFB diode laser, we obtain a satisfactory frequency precision, which was demonstrated from a quantitative measurement of the CO_2 spectrum at 1.6 μm. A sensitivity of 4×10^{-11} cm^{-1} Hz$^{-1/2}$ has been achieved using a RD cavity with a finesse of 1.5×10^5. Relatively simple structure, good quantitative capability, and very high sensitivity make the present instrument very suitable for trace gas detection applications. Since the linewidth of the RD cavity modes can be 1 kHz or less provided a RD cavity with improved thermal stability, it is possible to obtain spectra with kHz precision using MHz-linewidth lasers.

2. Experimental Setup

A diagram of the experimental setup is presented in Fig. 1(a). The laser beam from a DFB diode laser is sent into an acousto-optic modulator (AOM), and the first-order beam is coupled to a RD cavity with a finesse of about 1.5×10^5. A photodiode is used to detect the light emitted from the cavity. Once the detected signal reaches a preset threshold, a trigger signal is produced and the AOM is switched off for a few milliseconds. The RD signal is digitized and recorded by a fast digitizer (ADLink PCI-9846) installed in a personal computer. A fitting program based on the Levenberg–Marquardt algorithm is applied to fit the RD curve to an exponential decay function. The absorption coefficient α of the sample in the cavity can be determined from the decay time τ using the equation [18]

$$\frac{1}{c\tau(\nu)} = \alpha(\nu) - \frac{\ln R}{L} = \alpha(\nu) + \frac{1}{c\tau_0}, \qquad (1)$$

where c is the speed of light, ν is the laser frequency, L is the length of the cavity, R is the reflectivity of the cavity mirror, and τ_0 is the decay time of an empty cavity. Note that a higher reflectivity and longer cavity length will give a larger τ_0, which usually leads to a better sensitivity.

A. Spectral Scan: Matching the Cavity Modes One by One

The longitudinal modes of the RD cavity can be used as frequency markers to calibrate the spectrum provided that the cavity modes are sufficiently stable during a spectral scan. The frequency of a longitudinal mode of the cavity could be written as

$$\nu_N = \nu_0 + N \times \mathrm{FSR}, \tag{2}$$

where N is the index of the cavity modes and ν_0 is the frequency of the starting mode. The FSR value can be either calculated from the length of the RD cavity or derived from the recorded spectrum using the known frequencies of some molecular lines. Calibration using the cavity itself as a Fabry–Péret etalon has been applied in previous studies, for example, in Refs. [32,34,39,40], but in practice, it is not easy to assign a correct index to every selected cavity mode during a spectral scan. We attempted to scan the laser passing the cavity modes one by one, using a procedure similar to that given in Ref. [32]. The operating temperature of the laser diode was step-scanned by a controller (Fig. 1) with a resolution of 1 mK, equivalent to a frequency resolution of about 12 MHz. A triangle wave was applied to the injecting current (Fig. 1), modulating the laser frequency to match the corresponding cavity mode. The amplitude of the modulation is set to be well below the FSR value (typically 1/4 FSR), in order to pick only one cavity mode in a period. It was designed to record 20 RD data at each cavity mode. However, as shown in Fig. 2(a), there were quite a few events of mismatching during the scan. A mismatching event leads to a data point with a wrong index (N number), and therefore errors in the calibration. If such data points with wrong indices are in the vicinity of a line, it results in a considerably large deviation in the "observed" line width. For example, the mismatching events shown in Fig. 2(a) make the recorded line fictitiously wider than the true one, which is shown in Fig. 2(b).

Possible reasons for mismatching include frequency changes in the cavity modes, occasional resonances of the high-order spacial modes of the cavity, and jittering in the laser frequency. We put the RD cavity on a vibration-isolating plate and cover it with foam about 3 cm thick for thermoisolation, in order to reduce the temperature drift or mechanical vibrations. It may also help to reduce the influence from surrounding sound sources. The short-term temperature fluctuation of the cavity is reduced to about 0.01 K, and the resulting relative frequency change of the cavity modes should be on the order of 10^{-8} or less during a scan (typically 1 min). We can observe a long-term temperature drift following with the environment, but it only changes the starting point of individual scans (to be discussed later). The high-reflectivity (HR) mirrors are placed inside the sample cell and two antireflective windows are used to separate the sample gas and the ambient air. As a result, there is no pressure difference between both sides of the HR mirrors, which also reduces the elastic distortions due to changes of pressure either inside or outside the cell. We have also carefully aligned the laser beams and confirmed that the amplitudes of the resonances due to high-order spatial modes should be no more than a few percent of that of the zero-order mode and well below the threshold used to trigger the RD data acquisition.

A control program is applied to control the laser wavelength during the spectral scan (by controlling the injection current and operating temperature applied on the laser diode). The diagram given in Fig. 1(b) shows how it works when trying to record

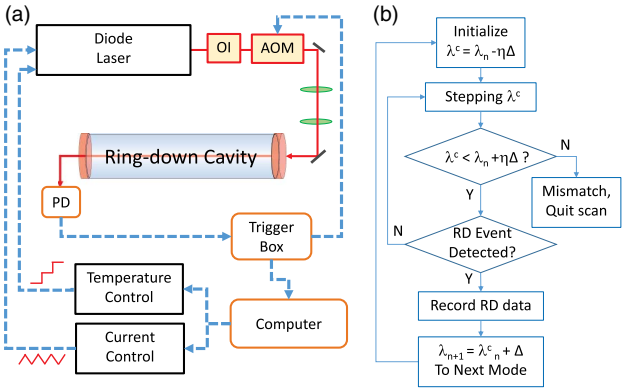

Fig. 1. (a) Configuration of the experimental setup. AOM, acousto-optic modulator; OI, optical isolator; PD, photodiode detector. (b) Control diagram for a strict mode-by-mode scan. λ^c, current wavelength of the diode laser; λ_n, wavelength of the nth mode of the cavity; Δ, wavelength difference between two adjacent modes of the cavity; η, control parameter, typically $0 < \eta < 0.3$. See text for details.

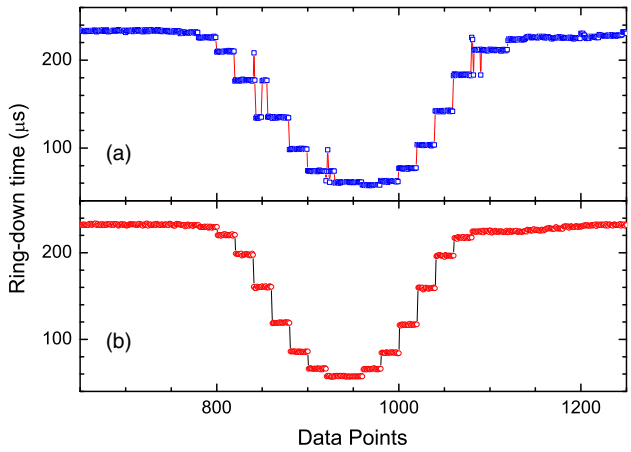

Fig. 2. Spectrum around an absorption line recorded (a) with and (b) without occurrences of mismatching. Twenty RD data were recorded on each cavity mode.

the RD data at the nth mode of the cavity. In general, it steps the laser wavelength within a preset region around the wavelength λ_n. λ_n is calculated with the "matching point" (laser diode temperature and current) of previous cavity mode λ_{n-1}, the FSR value of the cavity, and the producer-provided parameters of the laser diode. The width of the region is set to be $\eta\Delta$, where Δ is the difference in wavelength between two adjacent modes of the cavity and η is a control factor, which should be $0 < \eta < 0.5$. Abnormal changes in the recorded matching points indicate the occurrence of mismatching events. Any scan with mismatching events will be abandoned. It is critical to choose a proper value of η: (1) It should be sufficiently large. Because the control of the laser wavelength through operating temperature and injection current is inaccurate, a very narrow searching region increases the possibility of losing matching between the laser frequency and the target cavity mode. (2) It should be small to avoid the occurrence of mismatching. In our case, using η of 0.2 together with a modulation of the laser frequency with an amplitude of 25% of the FSR, we can step-scan the laser frequency from one cavity mode to the next one with correct indices. In this case, only scans confirmed to be with no occurrence of mismatching will be recorded and all the obtained data points in a spectrum have correct indices of the cavity modes. A piece of the recorded spectrum (20 repeated RD data on each step) is shown in Fig. 2(b).

B. Self-Calibration of the Spectrum

In order to verify the calibration and precision of the spectrometer, the CO_2 spectrum near 6391.7 cm^{-1} has been repeatedly measured for about 7 h and 320 spectra were recorded. The absorption lines within this region have been reported in Refs. [41,42] and included in the HITRAN database [43]. A simulated spectrum is shown in Fig. 3 (upper panel). By fitting the recorded spectrum using a multipeak fitting program, parameters of 10 lines shown in Fig. 3 were derived. Positions of the six strongest lines were used to calibrate the spectrum by a linear fit according to Eq. (2) using the frequencies given in HITRAN. The FSR and ν_0 values derived from each spectrum are presented in Fig. 4. The obtained FSR value is 115.45 ± 0.06 MHz, corresponding to a cavity length of 129.83 ± 0.06 cm, agreeing well with the directly measured length of 130.2 ± 0.3 cm. Note that there are altogether 131 data points in a spectrum (Fig. 3), which represent 131 cavity modes within the scan range. Any occurrence of data with wrong indices (mismatching) will result with a relative deviation of 1/131 (≈0.8%) on the obtained FSR. As a comparison, the maximum relative deviation shown in Fig. 4(a) is only 0.2%. It indicates that the data points in the recorded spectrum precisely match each of the cavity modes. Therefore, the spectrum can be readily calibrated using the FSR of the cavity.

However, slow frequency drift of the absolute frequencies of the cavity modes are inevitable in the measurements. This can be clearly seen from the variation of the ν_0 values shown in Fig. 4(b). The frequency fluctuation may comes from the change of cavity length due to the drift of the environmental temperature. We can notice that the typical change between two succeeding scans is on the order of 0.01 GHz (3×10^{-4} cm^{-1}). Some sudden "hopping" of about 0.1 GHz can also been found in Fig. 4(b). Since it coincides with the FSR value, the "hopping" is probably a result of a different cavity mode being selected when the scan started. Fluctuations of ν_0 lead to frequency shifts among the spectra recorded in different scans, on the order of 0.1 GHz (0.003 cm^{-1}). Although the shift is well below the Doppler width of a molecular line in this spectral range

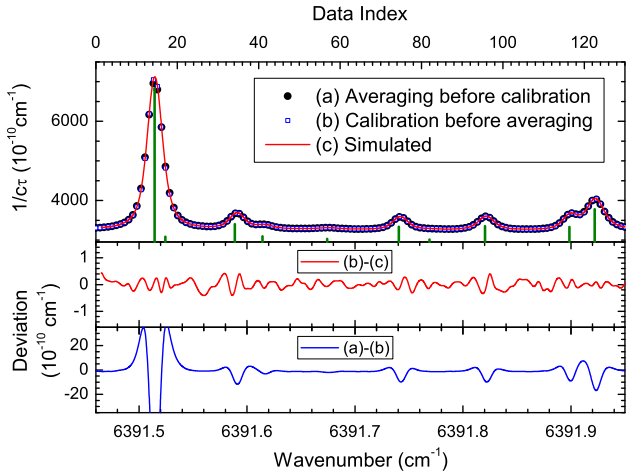

Fig. 3. Recorded and simulated spectrum near 6391.7 cm^{-1}. CO_2 sample pressure: 50 Torr. Upper panel: (a) solid circles, directly averaging 320 spectra according to the data indices; (b) open squares, averaging after each spectrum has been calibrated separately; (c) continuous line, simulated spectrum. The molecular lines included in the simulation are indicated with sticks. Water vapor presents in the sample as impurity, and two water lines at 6391.673 and 6391.770 cm^{-1} are included. The middle and bottom panels show the difference spectrum of (b)–(c) and (a)–(b), respectively.

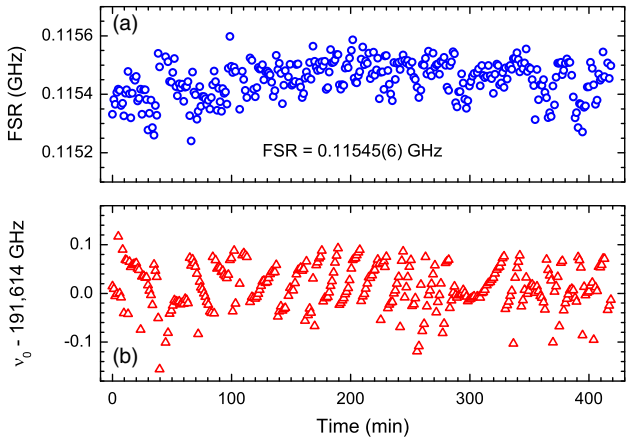

Fig. 4. FSR of the RD cavity and the frequency of the starting mode of the spectral scan [ν_0, see Eq. (2)] obtained from 320 spectra recorded in 7 h.

(0.012 cm^{-1} for CO_2), it reduces the precision of the obtained spectrum. In the upper panel of Fig. 3, two "averaged" experimental spectra are presented: (a) simply averaging the data according to the data index, and (b) averaged after each spectrum was calibrated separately. A simulated spectrum (c) is also given for comparison. The residuals between (b) and (c) indicate that the noise level of the averaged spectrum (b) is about 2×10^{-11} cm^{-1}. However, the difference spectrum between (a) and (b) presented in the figure shows clear structures around the absorption lines. It indicates that the lines in spectrum (a) are broadened, because the difference in ν_0 among the recorded spectra has not been considered before averaging. Calibration taking into account the shift in each scan will avoid the loss in precision, but we need at least one line with good signal-to-noise ratio in the spectrum.

C. Sensitivity and the Detection Limit

The sensitivity of a CRDS instrument is primarily limited by the noise in measured cavity loss. In order to evaluate the noise level of the present apparatus, the decay time at a fixed wavelength has been continuously measured. The measured cavity loss $(1/c\tau)$ and the corresponding Allan deviation are shown in Fig. 5. The noise level is at 4×10^{-11} cm^{-1} $Hz^{-1/2}$, and it reaches a MDAC of 6×10^{-12} cm^{-1} after an averaging time of about 60 s. Slow variation of the RD time prevents further improvements of the sensitivity by averaging more RD events. There have been discussions [20,23,30] on the possible reasons that may induce the drift, including mechanical deformation, temperature drift, high-order spatial mode excitation, external cavities coupled to the high-finesse cavity, and polarization dependence of the HR mirrors.

In practice, one needs to scan the laser to obtain a spectrum for quantitative measurements. Averaging the spectra obtained from repeated scans instead of accumulating RD events at fixed wavelengths can overcome the drifting baseline problem, but one must carefully align the cavity to avoid the etalon effects due to parasitic cavities beside the main high-finesse cavity. We evaluate the sensitivity of the present instrument by measuring the spectrum near 6218 cm^{-1}, where a CO_2 line is sitting in this region. The RD cavity has been continuously pumped by a dry scroll pump to mimic a gas sample containing trace CO_2. The total pressure of the residual air in the RD cavity was about 1 Pa. The spectrum with a width of about 0.3 cm^{-1} was recorded once a minute. The recorded spectra were coadded and the averaged spectra with averaging numbers of $N = 1$, 4, 16, 64, and 144 are shown in Fig. 6(a). A weak absorption line becomes more visible when the averaging number increases. This is the P(12) line of the $3\nu_1 + \nu_3$ band of $^{12}C^{16}O_2$ at 6218.089 cm^{-1}, with a line intensity of 1.492×10^{-23} $cm^{-1}/(\text{molecule cm}^{-2})$. The integral of the absorption line shows that the partial pressure of CO_2 in the RD cell was 2×10^{-3} Pa. The noise-equivalent MDAC, $\alpha_{\min}$, can be derived from each spectrum with different averaging number N. The results are shown in Fig. 6(b). The $\alpha_{\min}$ value decreases with increasing N, roughly proportional to $N^{-1/2}$. A MDAC of 5×10^{-12} cm^{-1} was achieved when about 100 spectra recorded in 2 h were included. As a comparison, Kassi and Campargue [23] obtained a MDAC of 5×10^{-13} cm^{-1} by averaging 6220 spectra recorded in 4.5 days, which is the best reported sensitivity obtained with CRDS. Note that a RD cavity with a finesse of 4×10^5 was used in that work, about three times the one used in the present work.

The detection limit of a target molecule can be directly calculated from the MDAC $\alpha_{\min}$ using the equation

$$P_{\min} = \frac{RT}{IN_A\phi_0}\alpha_{\min}, \tag{3}$$

where I is the line intensity in $cm^{-1}/(\text{molecule cm}^{-2})$, T is the temperature of the gas sample, N_A is the Avogadro constant, R is the molar gas constant, and ϕ_0 (in cm) is the height of the normalized line profile. In the case of Gaussian line profile, $\phi_0 = (\omega\sqrt{\pi})^{-1}$, where ω is the Gaussian width

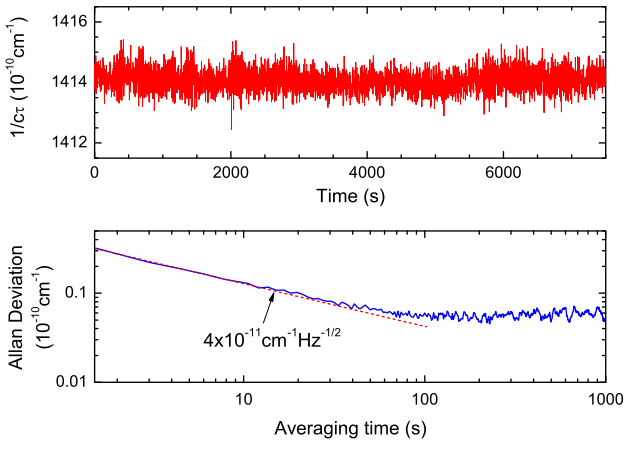

Fig. 5. Cavity loss $(1/c\tau)$ of an empty RD cavity (upper panel) and the Allan deviation (lower panel).

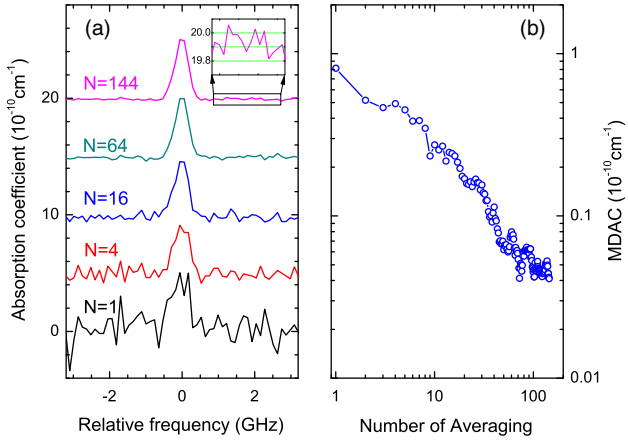

Fig. 6. CO_2 line at 6218.089 cm^{-1}. (a) Spectra with different averaging numbers. (b) MDAC obtained from spectra with different averaging numbers.

(1/e). If the 6218.089 cm^{-1} line shown in Fig. 6 is used for detecting CO_2 at a temperature of 296 K, the α_{min} value of 5×10^{-12} cm^{-1} corresponds to a CO_2 detection limit of 1.5×10^{-5} Pa.

3. Example of Quantitative Analysis: CO_2 Concentration in N_2

The quantitative accuracy of the instrument has been further verified by measuring the CO_2 concentrations in different nitrogen gas samples. The samples with different concentrations of carbon dioxide in nitrogen were prepared in the National Institute of Metrology (NIM, China) using the standard gravimetric method (GM). The nitrogen gas sample was purchased from Air Products with a stated purity of 99.999%. The carbon dioxide gas sample was purchased from China LvLing Gas Company with a stated purity also of 99.999%. The applied balance capacity is 10 Kg with a resolution of 1 mg (Mettler Toledo ID7). Two samples were prepared by the GM method, one with CO_2 concentration of 998.8 ± 1.0 μmol/mol, and the other of 348.9 ± 0.7 μmol/mol.

The CO_2 line at 6207.246 cm^{-1} was selected in the CRDS measurements. It is the P(24) line in the $3\nu_1 + \nu_3$ band of $^{12}C^{16}O_2$, with a line intensity of 1.295×10^{-23} $cm^{-1}/(molecule\ cm^{-2})$ at 296 K given in the HITRAN database [43]. The recorded spectrum was directly calibrated with the FSR of the RD cavity. The partial pressure of CO_2 in the RD cavity can be determined from the integral of the measured absorption coefficient:

$$P = \frac{RT \int \alpha(\nu) d\nu}{IN_A}. \quad (4)$$

The total sample pressure was measured by a capacitance gauge (MKS 627B, accuracy of 0.12%). Therefore, the relative concentration of CO_2 in the sample was derived. The CRDS-determined CO_2 concentrations in these two samples are 999 ± 3 and 350 ± 2 μmol/mol, respectively. We also prepared a series of samples by mixing the GM samples and pure nitrogen gas, and measured the CO_2 concentrations with CRDS. The results are shown in Fig. 7. The values from both methods are in good agreement with deviations below 3 μmol/mol. Because either the error in the frequency (ν, x axis) or the error in the cavity loss ($1/c\tau$, y axis) will lead to a deviation in the determined integrated line strength, the excellent agreement between the CRDS and GM results indicates that a satisfactory quantitative accuracy has been achieved by the present CRDS instrument.

As a demonstration of the trace detection capability, the instrument was applied to determine trace CO_2 concentration in pure nitrogen. The nitrogen gas (Nanking Special Gas Inc.) continuously passed through the sample cell with a flow rate of about 100 mL/min. The N_2 pressure in the cell was maintained to be 170 Torr and the spectrum of CO_2 near 6218 cm^{-1} was recorded to determine the CO_2 concentration. Since the previous gas sample in the cell has a higher CO_2 concentration, the detected CO_2 concentration is decreasing when we flush the cell with nitrogen gas, and finally it reaches a steady value which is believed to be the CO_2 concentration in the nitrogen gas. Figure 8(a) shows the spectrum recorded in a single scan when we just started flushing the cell. Figure 8(c) gives the spectrum of the sample after

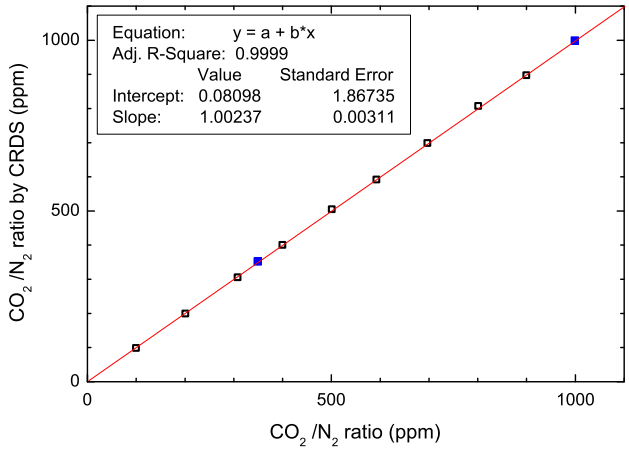

Fig. 7. CO_2 concentration in N_2 determined by CRDS. Samples shown with solid squares were prepared in NIM (Beijing) using the standard GM. Other samples shown with open squares were prepared in Hefei by mixing the GM samples with pure nitrogen gas.

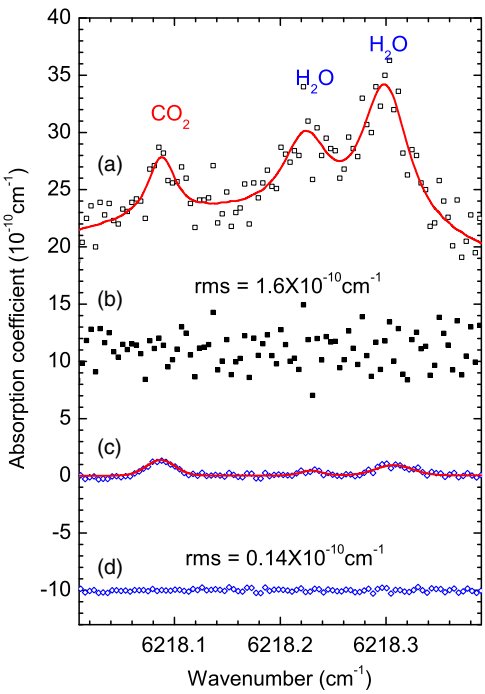

Fig. 8. Detection of trace CO_2 in pure nitrogen. (a) Observed spectrum (open squares) recorded before flushing the sample cell; single scan. The continuous curve is the simulated spectrum (CO_2, 0.5 ppmv; H_2O, 305 ppmv). (b) Differences between the observed and simulated spectra shown in (a). (c) Observed spectrum (open circles) recorded after flushing the sample cell with pure nitrogen, averaged from 204 scans. The continuous curve is the simulated spectrum (CO_2, 0.073 ppmv; H_2O, 12 ppmv). (d) Differences between the observed and simulated spectra shown in (c).

flushing the cell, which is averaged from 204 scans accumulated in about 2 h. Figures 8(b) and 8(d) are the corresponding fitting residuals, with root-mean-square deviations of 1.6×10^{-10} and 1.4×10^{-11} cm^{-1}, respectively. Besides the CO_2 line mentioned above, two H_2O lines have been included in the fitting. They are given in the HITRAN database [43], one at 6218.2305 cm^{-1} with a line intensity of 4.841×10^{-26} cm/molecule, and the other one at 6218.3018 cm^{-1} with a line intensity of 7.867×10^{-26} cm/molecule. The concentrations of CO_2 and H_2O have been determined from the observed spectrum according to Eq. (4). Before flushing [Fig. 8(a)], the CO_2 and H_2O concentrations were 0.50 and 305 ppmv, respectively. After flushing [Fig. 8(c)], the CO_2 concentration decreased to 73 ± 7 ppbv, while the H_2O concentration decreased to 12 ± 2 ppmv. The fitting residual shown in Fig. 8(d) corresponds to a CO_2 detection limit of 7 ppbv. As a comparison, in some recent studies, the reported detection limits of CO_2 are 40 ppbv by a laser absorption spectrometer based on a tunable quantum cascade laser operating at 4.3 μm [44], and 9 ppbv by a chromatographic method [45]. The spectrometer presented here has a high sensitivity, is relatively simple, and does not require cryogenic cooling for either lasers or detectors.

4. Discussion

We have presented a cw cavity RD spectrometer employing the "scanning laser" method, in which the frequency of a relatively broad linewidth DFB diode laser is swept to match narrow longitudinal modes of a high-finesse RD cavity. A control scheme is applied to scan the diode laser frequency in a stepwise way, ensuring that the data are taken at the frequencies on resonance with the cavity modes in sequence; therefore, the recorded spectrum can be directly calibrated using the data indices and the FSR of the cavity. Using a fibered DFB laser at 1.6 μm and a RD cavity with a finesse of 1.5×10^5, we obtained a sensitivity of 4×10^{-11} cm^{-1} Hz$^{-1/2}$. By measuring a piece of spectrum 0.5 cm^{-1} wide involving several CO_2 lines, we determined the FSR of the cavity with an accuracy of 0.06 MHz (relatively 0.05%), which allows analysis with satisfactory quantitative accuracy. As a demonstration, the instrument has been applied to determine CO_2 concentrations in nitrogen gases. A CO_2 detection limit of 1.5×10^{-5} Pa has been achieved by averaging about 100 spectra obtained in 2 h. We have also applied the same setup for trace moisture detection using a DFB laser at 1.39 μm. A similar sensitivity has been obtained. By detecting the $H_2^{16}O$ line at 7168.437 cm^{-1}, which has a line intensity of 1.17×10^{-20} cm^{-1}/(molecule cm^{-2}), about 800 times stronger than the CO_2 line at 6218 cm^{-1}, we obtained a detection limit for water vapor of 2×10^{-8} Pa, or a molecular density of 5×10^6 molecules/cm^3.

Locking the RD cavity length to an external frequency standard can improve the frequency precision and reproducibility [37], but the method applied in this work is comparably simpler, which could be more easily employed in most applications. It is also worth noting that the frequency precision is in principle only limited by the stability of the cavity mode. We can expect a much better frequency accuracy if using a RD cavity made of low-expansion material and implementing a better thermostabilized chamber. Such high-precision CRDS can be even realized with broad-linewidth lasers, only requiring that the laser linewidth is narrower than the FSR of the cavity. The present method may help to extend precision spectroscopy to those spectral regions lacking narrow-linewidth lasers. High-precision CRDS implementing a cavity with a long-term thermostability of better than 1 mK is under construction in our laboratory [46], which can be potentially applied as a Doppler broadening thermometry (DBT) [47,48]. Compared to the recent DBT study [49] using direct absorption spectroscopy, the superior sensitivity of CRDS will allow measurements with lower sample gas pressures, which may reduce the uncertainty in the line profile due to pressure-broadening effects [50]. Another potential application of such a CRDS instrument with better temperature stability is the precise determination of the concentration of multi-substituted isotopologues ("clumped-isotope") [51], which attracts increasing interest in geosciences.

This work is jointly supported by the NBRPC (2013BAK12B00 and 2013CB834602) and the NSFC (91221304 and 21225314).

References

1. M. N. Fiddler, I. Begashaw, M. A. Mickens, M. S. Collingwood, Z. Assefa, and S. Bililign, "Laser spectroscopy for atmospheric and environmental sensing," Sensors **9**, 10447–10512 (2009).
2. J. S. Li, W. Chen, and H. Fischer, "Quantum cascade laser spectrometry techniques: a new trend in atmospheric chemistry," Appl. Spectrosc. Rev. **48**, 523–559 (2013).
3. C. Wang and P. Sahay, "Breath analysis using laser spectroscopic techniques: breath biomarkers, spectral fingerprints, and detection limits," Sensors **9**, 8230–8262 (2009).
4. R. K. Hanson, "Applications of quantitative laser sensors to kinetics, propulsion and practical energy systems," Proc. Combust. Inst. **33**, 1–40 (2011).
5. U. Willer and W. Schade, "Photonic sensor devices for explosive detection," Anal. Bioanal. Chem. **395**, 275–282 (2009).
6. M. W. Sigrist, R. Bartlome, D. Marinov, J. M. Rey, D. E. Vogler, and H. Waechter, "Trace gas monitoring with infrared laser-based detection schemes," Appl. Phys. B **90**, 289–300 (2008).
7. A. Elia, P. M. Lugara, C. Di Franco, and V. Spagnolo, "Photoacoustic techniques for trace gas sensing based on semiconductor laser sources," Sensors **9**, 9616–9628 (2009).
8. G. Wysocki, R. Lewicki, R. F. Curl, F. K. Tittel, L. Diehl, F. Capasso, M. Troccoli, G. Hofler, D. Bour, S. Corzine, R. Maulini, M. Giovannini, and J. Faist, "Widely tunable mode-hop free external cavity quantum cascade lasers for high resolution spectroscopy and chemical sensing," Appl. Phys. B **92**, 305–311 (2008).
9. S. M. Cristescu, S. T. Persijn, S. T. L. Hekkert, and F. J. M. Harren, "Laser-based systems for trace gas detection in life sciences," Appl. Phys. B **92**, 343–349 (2008).
10. G. Duxbury, N. Langford, M. T. McCulloch, and S. Wright, "Quantum cascade semiconductor infrared and far-infrared lasers: from trace gas sensing to non-linear optics," Chem. Soc. Rev. **34**, 921–934 (2005).
11. D. D. Arslanov, S. M. Cristescu, and F. J. M. Harren, "Optical parametric oscillator based off-axis integrated cavity output

spectroscopy for rapid chemical sensing," Opt. Lett. **35**, 3300–3302 (2010).
12. J. B. Barria, S. Roux, J.-B. Dherbecourt, M. Raybaut, J.-M. Melkonian, A. Godard, and M. Lefebvre, "Microsecond fiber laser pumped, single-frequency optical parametric oscillator for trace gas detection," Opt. Lett. **38**, 2165–2167 (2013).
13. D. Richter, A. Fried, and P. Weibring, "Difference frequency generation laser based spectrometers," Laser Photon. Rev. **3**, 343–354 (2009).
14. F. Adler, M. J. Thorpe, K. C. Cossel, and J. Ye, "Cavity-enhanced direct frequency comb spectroscopy: technology and applications," Annu. Rev. Anal. Chem. **3**, 175–205 (2010).
15. C. Wang, N. Srivastava, B. A. Jones, and R. B. Reese, "A novel multiple species ringdown spectrometer for *in situ* measurements of methane, carbon dioxide, and carbon isotope," Appl. Phys. B **92**, 259–270 (2008).
16. S. S. Brown, "Absorption spectroscopy in high-finesse cavities for atmospheric studies," Chem. Rev. **103**, 5219–5238 (2003).
17. A. Okeefe and D. A. G. Deacon, "Cavity ring-down optical spectrometer for absorption-measurements using pulsed laser sources," Rev. Sci. Instrum. **59**, 2544–2551 (1988).
18. P. Zalicki and R. N. Zare, "Cavity ring-down spectroscopy for quantitative absorption measurements," J. Chem. Phys. **102**, 2708–2717 (1995).
19. J. B. Dudek, P. B. Tarsa, A. Velasquez, M. Wladyslawski, P. Rabinowitz, and K. K. Lehmann, "Trace moisture detection using continuous-wave cavity ring-down spectroscopy," Anal. Chem. **75**, 4599–4605 (2003).
20. H. Huang and K. K. Lehmann, "Long-term stability in continuous wave cavity ringdown spectroscopy experiments," Appl. Opt. **49**, 1378–1387 (2010).
21. B. Gao, W. Jiang, A.-W. Liu, Y. Lu, C.-F. Cheng, G.-S. Cheng, and S.-M. Hu, "Ultra sensitive near-infrared cavity ring down spectrometer for precise line profile measurement," Rev. Sci. Instrum. **81**, 043105 (2010).
22. A. Cygan, D. Lisak, P. Maslowski, K. Bielska, S. Wojtewicz, J. Domyslawska, R. S. Trawinski, R. Ciuryło, H. Abe, and J. T. Hodges, "Pound–Drever–Hall-locked, frequency-stabilized cavity ring-down spectrometer," Rev. Sci. Instrum. **82**, 063107 (2011).
23. S. Kassi and A. Campargue, "Cavity ring down spectroscopy with 5×10^{-13} cm^{-1} sensitivity," J. Chem. Phys. **137**, 234201 (2012).
24. G. W. Truong, K. O. Douglass, S. E. Maxwell, R. D. van Zee, D. F. Plusquellic, J. T. Hodges, and D. A. Long, "Frequency-agile, rapid scanning spectroscopy," Nat. Photonics **7**, 532–534 (2013).
25. D. Romanini, J. Gambogi, and K. K. Lehmann, "Cavity ring-down spectroscopy with CW diode laser excitation," in *Proceedings of 50th International Symposium on Molecular Spectroscopy* Columbus, Ohio (1995).
26. D. Romanini, A. A. Kachanov, N. Sadeghi, and F. Stoeckel, "Cw cavity ring down spectroscopy," Chem. Phys. Lett. **264**, 316–322 (1997).
27. B. A. Paldus, C. C. Harb, T. G. Spence, B. Willke, J. Xie, J. S. Harris, and R. N. Zare, "Cavity-locked ring-down spectroscopy," J. Appl. Phys. **83**, 3991–3997 (1998).
28. J. Morville, D. Romanini, A. A. Kachanov, and M. Chenevier, "Two schemes for trace detection using cavity ringdown spectroscopy," Appl. Phys. B **78**, 465–476 (2004).
29. B. A. Paldus and A. A. Kachanov, "An historical overview of cavity-enhanced methods," Can. J. Phys. **83**, 975–999 (2005).
30. H. F. Huang and K. K. Lehmann, "Noise in cavity ring-down spectroscopy caused by transverse mode coupling," Opt. Express **15**, 8745–8759 (2007).
31. H. Pan, C.-F. Cheng, Y. R. Sun, B. Gao, A.-W. Liu, and S.-M. Hu, "Laser-locked, continuously tunable high resolution cavity ring-down spectrometer," Rev. Sci. Instrum. **82**, 103110 (2011).
32. K. J. Schulz and W. R. Simpson, "Frequency-matched cavity ring-down spectroscopy," Chem. Phys. Lett. **297**, 523–529 (1998).
33. N. J. van Leeuwen, J. C. Diettrich, and A. C. Wilson, "Periodically locked continuous-wave cavity ringdown spectroscopy," Appl. Opt. **42**, 3670–3677 (2003).
34. B. J. Orr and Y. He, "Rapidly swept continuous-wave cavity-ringdown spectroscopy," Chem. Phys. Lett. **512**, 1–20 (2011).
35. J. T. Hodges and D. Lisak, "Frequency-stabilized cavity ring-down spectrometer for high-sensitivity measurements of water vapor concentration," Appl. Phys. B **85**, 375–382 (2006).
36. D. W. Chandler and K. E. Strecker, "Dual-etalon frequency-comb cavity ringdown spectrometer," J. Chem. Phys. **136**, 154201 (2012).
37. J. T. Hodges, H. P. Layer, W. W. Miller, and G. E. Scace, "Frequency-stabilized single-mode cavity ring-down apparatus for high-resolution absorption spectroscopy," Rev. Sci. Instrum. **75**, 849–863 (2004).
38. J. T. Hodges and R. Ciuryło, "Automated high-resolution frequency-stabilized cavity ring-down absorption spectrometer," Rev. Sci. Instrum. **76**, 023112 (2005).
39. H. S. Margolis, G. Huang, G. P. Barwood, S. N. Lea, H. A. Klein, W. R. C. Rowley, P. Gill, and R. S. Windeler, "Absolute frequency measurement of the 674 nm $^{88}Sr^{+}$ clock transition using a femtosecond optical frequency comb," Phys. Rev. A **67**, 032501 (2003).
40. M. J. Thorpe and J. Ye, "Cavity-enhanced direct frequency comb spectroscopy," Appl. Phys. B **91**, 397–414 (2008).
41. Y. Ding, P. Macko, D. Romanini, V. I. Perevalov, S. A. Tashkun, J. L. Teffo, S. M. Hu, and A. Campargue, "High sensitivity cw-cavity ringdown and Fourier transform absorption spectroscopies of $^{13}CO_2$," J. Mol. Spectrosc. **226**, 146–160 (2004).
42. B. V. Perevalov, S. Kassi, D. Romanini, V. I. Perevalov, S. A. Tashkun, and A. Campargue, "Cw-cavity ringdown spectroscopy of carbon dioxide isotopologues near 1.5 μm," J. Mol. Spectrosc. **238**, 241–255 (2006).
43. L. S. Rothman, I. E. Gordon, Y. Babikov, A. Barbe, D. Chris Benner, P. F. Bernath, M. Birk, L. Bizzocchi, V. Boudon, L. R. Brown, A. Campargue, K. Chance, E. A. Cohen, L. H. Coudert, V. M. Devi, B. J. Drouin, A. Fayt, J. M. Flaud, R. R. Gamache, J. J. Harrison, J. M. Hartmann, C. Hill, J. T. Hodges, D. Jacquemart, A. Jolly, J. Lamouroux, R. J. Le Roy, G. Li, D. A. Long, O. M. Lyulin, C. J. Mackie, S. T. Massie, S. Mikhailenko, H. S. P. Mller, O. V. Naumenko, A. V. Nikitin, J. Orphal, V. Perevalov, A. Perrin, E. R. Polovtseva, C. Richard, M. A. H. Smith, E. Starikova, K. Sung, S. Tashkun, J. Tennyson, G. C. Toon, V. G. Tyuterev, and G. Wagner, "The HITRAN2012 molecular spectroscopic database," J. Quant. Spectrosc. Radiat. Transfer **130**, 4–50 (2013).
44. V. L. Kasyutich, D. Poulidi, M. Jalil, I. S. Metcalfe, and P. A. Martin, "Application of a cw quantum cascade laser CO_2 analyser to catalytic oxidation reaction monitoring," Appl. Phys. B **110**, 263–269 (2013).
45. M. J. van Rensburg, A. Botha, and E. Rohwer, "Analysis of trace amounts of carbon dioxide, oxygen and carbon monoxide in nitrogen using dual capillary columns and a pulsed discharge helium ionisation detector," J. Chromatogr. A **1167**, 102–108 (2007).
46. Y. R. Sun, H. Pan, C.-F. Cheng, A.-W. Liu, J.-T. Zhang, and S.-M. Hu, "Application of cavity ring-down spectroscopy to the Boltzmann constant determination," Opt. Express **19**, 19993–20002 (2011).
47. C. Daussy, M. Guinet, A. Amy-Klein, K. Djerroud, Y. Hermier, S. Briaudeau, C. J. Bordé, and C. Chardonnet, "Direct determination of the Boltzmann constant by an optical method," Phys. Rev. Lett. **98**, 250801 (2007).
48. G. Casa, A. Castrillo, G. Galzerano, R. Wehr, A. Merlone, D. DiSerafino, P. Laporta, and L. Gianfrani, "Primary gas thermometry by means of laser-absorption spectroscopy: determination of the Boltzmann constant," Phys. Rev. Lett. **100**, 200801 (2008).
49. L. Moretti, A. Castrillo, E. Fasci, M. D. De Vizia, G. Casa, G. Galzerano, A. Merlone, P. Laporta, and L. Gianfrani, "Determination of the Boltzmann constant by means of precision measurements of $H_2{}^{18}O$ line shapes at 1.39 μm," Phys. Rev. Lett. **111**, 060803 (2013).
50. A. Cygan, D. Lisak, R. S. Trawiński, and R. Ciuryło, "Influence of the line-shape model on the spectroscopic determination of the Boltzmann constant," Phys. Rev. A **82**, 032515 (2010).
51. J. M. Eiler, ""Clumped-isotope" geochemistry: the study of naturally-occurring, multiply-substituted isotopologues," Earth Planet. Sci. Lett. **262**, 309–327 (2007).